

# Basic mechanisms driving complex spike dynamics in a chemotaxis model with logistic growth.

Theodore Kolokolnikov\*, Juncheng Wei† and Adam Alcolado‡

October 5, 2013

## Abstract

We investigate Keller-Segel model with logistic self-production terms that exhibits complex spatio-temporal dynamics of spikes. These dynamics are driven by merging of spikes on one hand, and spike insertion on the other. In this paper we analyse the basic mechanisms that initiate and sustain these events. We identify two distinguished regimes. In the first regime, a single interior spike drifts towards a boundary. This instability is responsible for spike merging. The same regime further exhibits spike insertion; we identify a fold-point bifurcation which is precursor to spike insertion event. In the second regime, we show that it is possible to stabilize a single interior spike, and we compute analytically a critical threshold which is responsible for spike stabilization. In particular, our calculation characterizes a stable spike in the Keller-Segel model with logistic growth; this is in contrast to the classical Keller-Segel model where the interior spike is known to be unstable.

## 1 Introduction

Chemotaxis is the ability of micro-organisms or cells to sense and move in response to chemical gradients. Models of chemotaxis have a long history, starting with the seminal 1970 work by Keller and Segel [1, 2], in which they introduce what is now called the Keller-Segel model. This model consists of two PDE's which couple together the bacterial density and the concentration of the chemo-attractant. Keller-Segel system and its variants have been used in a wide variety of contexts, including modeling slime molds [1], bacterial colonies [3, 4, 5, 6], skin patterns [7, 8] and tumor formation [9] among others [10]. Quite aside from its biological relevance, the Keller-Segel model has been studied extensively by mathematicians because of its intrinsic mathematical beauty and its uncanny ability to generate very interesting and intriguing patterns. It is one of the simplest systems of PDE models that has very intricate solution structure but that is still accessible to a wide range of mathematical techniques, including the study of existence/uniqueness of solutions, blowup analysis, and pattern formation. There are literally hundreds of papers on various mathematical aspects of chemotaxis. See reviews [11, 12] and references therein.

The purpose of this paper is to study basic pattern formation in a model of chemotaxis with self-production terms. The model we consider is

$$u_t = D_u u_{xx} - \chi(uv_x)_x + ru(1 - u/K), \quad v_t = D_v v_{xx} + \alpha u - \beta v. \quad (1)$$

Here,  $u$  represents cell density and  $v$  represents the density of the chemoattractant. Cell population dynamics are modeled using the logistic production term  $ru(1 - u/K)$ ; the cross-diffusion term  $\chi(uv_x)_x$  model the sensing mechanism and cells diffuse with diffusion coefficient  $D_u$ . The chemo-attractant is excreted by the cells themselves at a rate  $\alpha u$ , decays at rate  $\beta v$ , and diffuses with diffusion coefficient  $D_v$ .

The “classical” Keller-Segel model corresponds to setting  $r = 0$  in (1). A large literature exists on the classical case; see [12] and references therein for an extensive overview. One of the main results for the classical Keller-Segel model is the presence of a *chemotactic collapse* in two dimensions, whereby the solution blows up in finite time at certain

---

\*Department of Mathematics and Statistics, Dalhousie University, Halifax, N.S., Canada. Email: tkolokol@mathstat.dal.ca

†Department of Mathematics, Chinese University of Hong Kong, Shatin, Hong Kong, and Department of Mathematics, University of British Columbia, Vancouver, B.C., Canada. wei@math.cuhk.edu.hk

‡Department of Mathematics, McGill university, adam.alcolado@mail.mcgill.ca

points of the domain, provided that the initial mass is sufficiently large. The chemotactic collapse, together with either formal asymptotic or rigorous constructions of the local blowup profile, has been studied by many authors. See for example [13, 14, 15, 16, 17, 18, 19] and many other references in [12]. The introduction of the logistic term prevents the chemotactic collapse and leads to very complex patterns.

Self-production terms were introduced in [20] and [7]. In particular (1) is a special case of the model considered in [7] which has a more general saturation term  $\alpha u/(\mu + u)$  instead of  $au$ . Generally speaking, saturation in the self-production terms acts to deter blowup and facilitates pattern formation [21, 22]. By now there is a large literature on chemotaxis with self-production. In [23] the authors considered a cubic growth term, i.e.  $u(1 - u/K)$  replaced by  $u(1 - u)(u - a)$ . They showed that in a certain regime the solution consists of several interfaces that separates regions (or phases) where  $u$  is either +1 or 0. They also analysed in detail the stability and evolution of these interface solutions in one and two dimensions. In [24, 22] the authors showed that phase-separation solution can also occur as a result of nonlinear sensing, for instance if  $\chi(uv_x)_x$  is replaced by  $\chi(u(1 - u)v_x)_x$ , even for a quadratic growth term. They also established global existence of solutions. Even without cubic nonlinearities or nonlinear sensing, equations (1) still generate complex patterns in the Turing-unstable regime [7, 25, 24, 22, 21]. However the solution in this case consists of *spikes*, such as shown in figure 1, and not of phase-separated interfaces. Spikes are small localized regions of high concentration of  $u$ , with relatively small concentrations of  $u$  elsewhere.

Even more interesting, as demonstrated numerically in [21, 24, 22], the addition of a logistic production term in (1) results in very complex and intriguing spike dynamics, such as spike merging, spike creation, oscillations and spatio-temporal chaos. This behaviour is not present in the classical Keller-Segel model. A typical simulation of this phenomenon is shown in Figure 1. The spikes in this simulation they tend to move towards each other and merge; on the other hand, new spikes are created when there is too much "free space" inbetween. In [26, 27] the authors showed the existence of a compact exponential attractor for (1). In [28] the authors computed numerically Lyapunov exponents and bifurcation diagram which indicates the presence of spatio-temporal chaos in the system. In [29], the authors perform a Turing-type analysis for the system (1). They show that the heterogeneous solutions bifurcate from a homogeneous state, and compute the amplitude of the solutions close to the bifurcation point. Unfortunately, this analysis does not capture the localized nature spikes, which exist in the fully nonlinear regime far from the homogeneous state. In a recent work [30], the authors model these dynamics by encoding merging/creation events into a dynamical system, where particles can be created or destroyed in a collision. This "high-level" system of particle dynamics reproduces the observed behaviour.

In this paper we address the following basic questions about the mechanisms underlying spike dynamics of (1):

1. What is the profile of the spike?
2. Why/when do the spikes move towards each-other?
3. What is the mechanism responsible for "spike insertion"?

We identify two distinguished parameter regimes and three distinct types of spike solutions with very different stability properties. The three solution types are:

- **Type I:** A single interior spike that is always unstable regardless of domain size and moves to the boundary without self-replication.
- **Type II:** Spike insertion is observed as domain size is increased.
- **Type III:** There exists a threshold such that a single interior spike is either stable or unstable.

We provide an analytical explanation for each of these three types of behaviour. Each solution type is constructed asymptotically. Then its stability is studied. As a result, this provides a characterization of the expected behaviour of the system within these regimes.

The contents of this paper are as follows. In section 2 we treat Type 1 solution. This is the simplest of the three types. The analysis is similar to what was done in [19] for the classical Keller-Segel system. There, the metastability of a spike was analysed; it was shown that for a classical Keller-Segel system in one dimension, an interior spike is metastable and as a result, will move very slowly towards the boundary of the domain. Whereas in the classical KS system the spike mass is determined by the mass of the initial conditions, for equations (1), the spike mass is independent of initial conditions and is determined instead by a balance between the growth  $ru$  and the saturation term  $-ru^2/K$ . Nonetheless, the stability analysis of type 1 solution follows the procedure developed in [19] and the end-result is similar: an interior spike is unstable due to exponentially small translational instabilities.

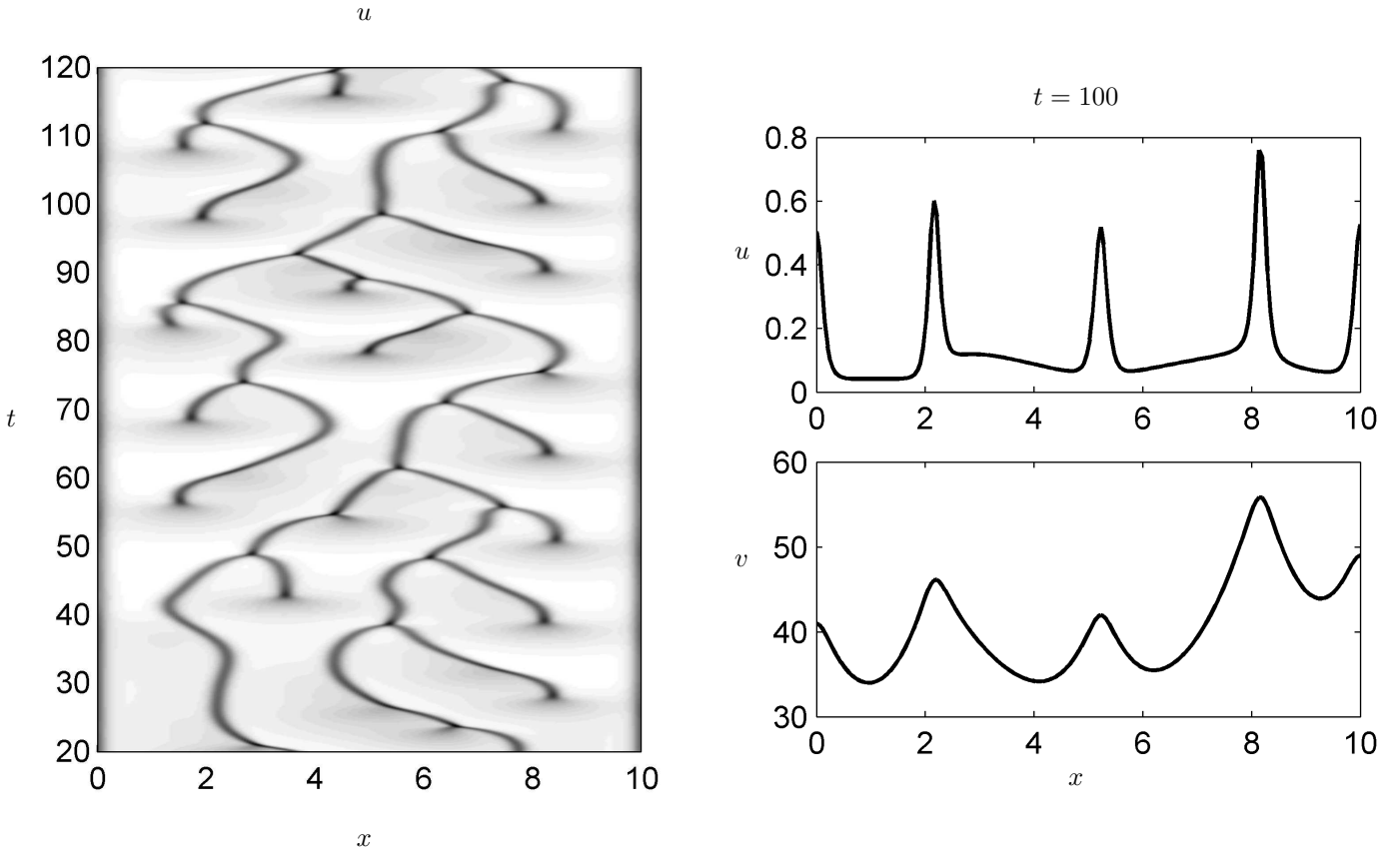


Figure 1: Left: numerical simulation of (2) on a domain of size 10 with  $\varepsilon = 0.05, a = 15$ . Contour plot of  $u$  in time and space is shown. Right: snapshot of the solution at  $t = 100$ . Software FlexPDE [31] was used for numerical simulations of the time-dependent system (2).

In section 3 we study type II solutions. We demonstrate that there is a critical threshold which leads to spike insertion as the parameters are varied past that threshold. This thresholding is due to the disappearance of the steady state at the fold point. In this sense, the mechanism for spike insertion is similar to self-replication such as studied in [32], [33]. This phenomenon has no analogue in the classical KS system.

In section 4 we derive the threshold for stability of type III solutions. This threshold is not present at all in the original KS model; in fact in the absence of the production terms, the spikes in the original KS model either merge or drift towards the boundary. On the other hand, the stability of an interior spike for system (1) was first observed numerically in [21]. This is the first time that such stability is explained analytically. The study of stabilizing mechanism requires a very delicate computation of an outer region.

## 2 Type I solutions

In this section, we consider the following regime, which is a rescaling of (1)<sup>1</sup>:

$$u_t = (\varepsilon u_x - uv_x)_x + u - u^2, \quad \tau v_t = v_{xx} + \frac{a}{\varepsilon} u - v \quad (2)$$

$$u_x(\pm L, t) = 0 = v_x(\pm L, t) \quad (3)$$

<sup>1</sup>Equations (2) are obtained from (1) via the following transformations, after dropping the \*'s:

$$u = Ku^*, \quad v = \frac{r}{\chi} v^*, \quad x = \sqrt{\frac{D_v}{\beta}} x^*, \quad t = \frac{1}{r} t^*$$

$$\varepsilon = D_u/r, \quad a = \frac{\alpha \chi D_u K}{\beta r^2}, \quad \tau = r/\beta,$$

with the assumptions that

$$0 < \varepsilon \ll 1; \quad a, \tau, L \text{ are positive and } O(1). \quad (4)$$

Biologically, this corresponds to small diffusion of cell density  $u$  (relative to the chemo-attractant  $v$  or to the chemotaxis-induced motion) and high chemo-attractant production by cells (relative to chemo-attractant decay rate)

In §2.1, we will first construct a steady which consists of a single spike for  $u$ , centered at the origin, whose width is of  $O(\varepsilon)$ . It turns out that there are two possible such solutions for the regime (2), which we refer to as type I and type II. Type I solution is such that  $u$  is exponentially small in the outer region  $|x| \gg O(\varepsilon)$  away from the spike. Type II solution, which is studied in §3, is more complicated and the outer region satisfies a certain third order ODE. In §2.2 we will study the stability of type I solution. There are two eigenvalues to consider, characterised by the parity (odd or even) of the corresponding eigenfunctions. We will show that the even eigenvalue is stable but the odd is unstable. The instability of the odd eigenvalue induces a translational motion of the spike; as a result, the spike moves towards the closest boundary until it merges with it.

Type II steady state is constructed in §3. We show that there exists a threshold  $a_c$  such that type II solutions do not exist for  $a < a_c$ ; this is unlike the type I solutions which exist for all  $a > 0$ .

## 2.1 Type I Steady state

We proceed to construct the steady state to (2) in the form of a symmetric spike centered at the origin. This is equivalent to constructing a half-spike on the half-interval  $[0, L]$  with Neumann boundary conditions. A sample profile for type I half-spike is illustrated in Figure 2(a) and corresponds to  $u$  being exponentially small in the outer region. From (2) the steady state equations on the half-domain  $x \in [0, L]$  are

$$(\varepsilon u_x - uv_x)_x + u - u^2 = 0, \quad 0 = v_{xx} + \frac{a}{\varepsilon}u - v \quad (5)$$

with Neumann boundary conditions for  $u, v$  at  $x = 0, L$ . The spike itself is located at  $x = 0$  and has an extent of  $O(\varepsilon)$ . To capture its profile, we introduce the inner variables as

$$\begin{aligned} x &= \varepsilon y \\ u &= U(y); \\ v &= v_0 + \varepsilon W(y) \end{aligned}$$

where  $v_0 = v(0)$  is to be determined (see (11) below), and  $W(0) = 0$ . Note that in the inner variables, the leading order equation for  $v$  reads  $v_{0yy} = 0$ . Combined with the assumption that  $v_{0y} = 0$  at  $y = 0$ , this implies that  $v_0$  is constant independent of  $y$ . In the inner variables we then obtain the problem

$$U_{yyy} - (UW_y)_y + \varepsilon(U - U^2) = 0; \quad W_{yy} + aU - (v_0 + \varepsilon W)\varepsilon = 0.$$

Next we expand the solution as

$$U = U_0 + \varepsilon U_1 \dots; \quad W = W_0 + \varepsilon W_1 + \dots$$

The leading order equations are

$$U_{0yy} - (U_0 W_{0y})_y = 0; \quad W_{0yy} + aU_0 = 0. \quad (6)$$

Recalling Neumann boundary conditions at  $y = 0$ , we therefore obtain

$$W_{0y} = \frac{U_{0y}}{U_0}; \quad \left(\frac{U_{0y}}{U_0}\right)_y + aU_0 = 0. \quad (7)$$

We seek solution to (7) with  $U_0(y) \rightarrow 0$  as  $y \rightarrow \infty$  and with  $U_{0y} = 0 = W_{0y}$  at  $y = 0$ . We obtain the solution

$$U_0 = \xi \operatorname{sech}^2\left(y\sqrt{\frac{\xi a}{2}}\right); \quad W_{0y} = -\sqrt{2\xi a} \tanh\left(y\sqrt{\frac{\xi a}{2}}\right) \quad (8)$$

where  $\xi$ , the height of the spike, is the free parameter that is due to the scaling invariance of the inner problem (6). To determine the height  $\xi$ , we now consider the outer region  $L > x \gg \varepsilon$ . There are two possible solutions which we shall call type I and type II.

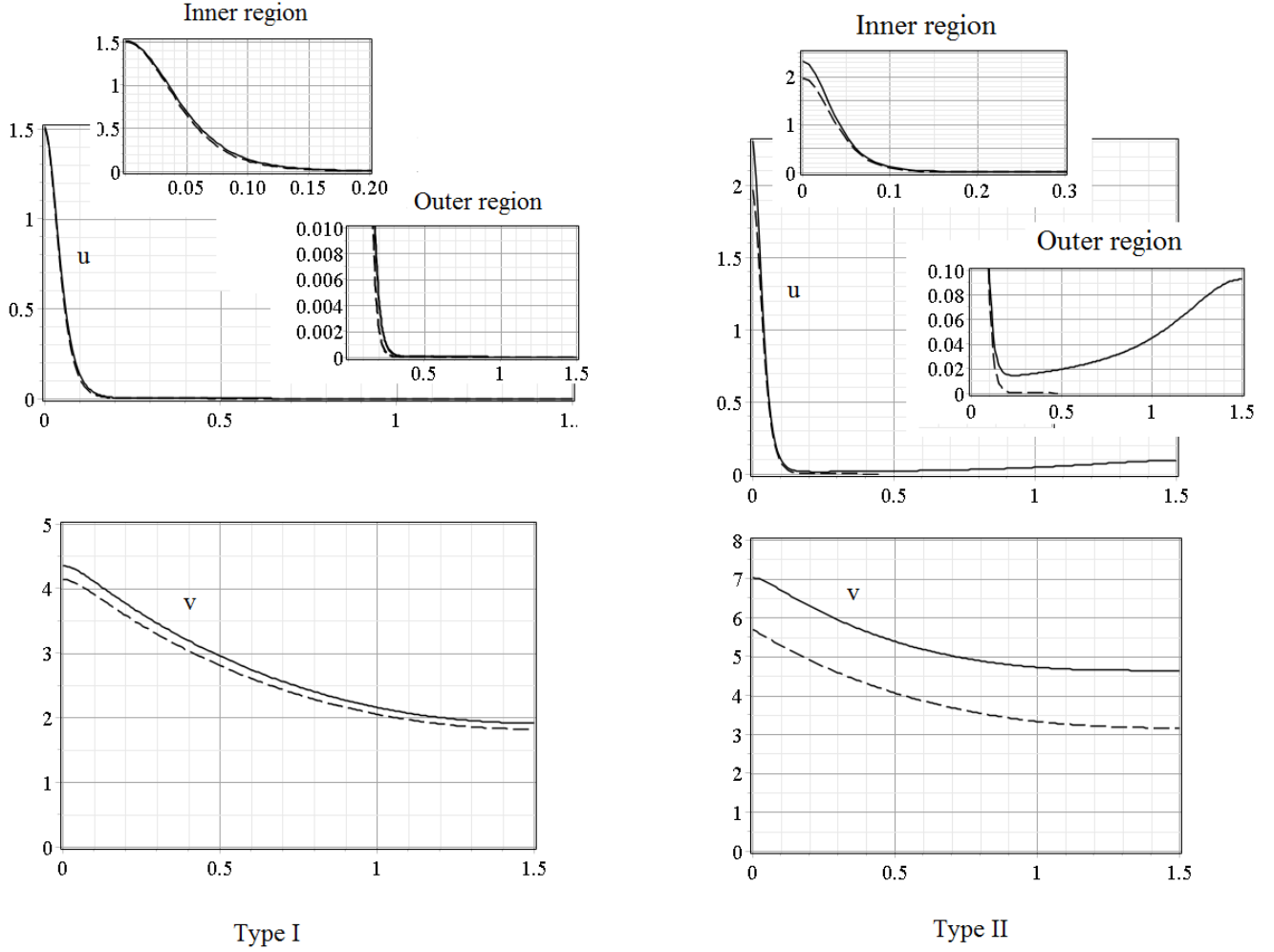


Figure 2: Two types of steady state solutions to (5). Parameter values are  $\varepsilon = 0.1, L = 1.5, a = 5$ . Solid curves are obtained by using Maple's numerical boundary value problem solver to solve (5). Dashed curves are asymptotic approximations as follows. Type I:  $u$  is exponentially small in the outer region. Dashed curve is the asymptotic solution given by (14) (for  $u$ ) and by (15) (for  $v$ ). Type II:  $u$  is of  $O(\varepsilon)$  in the outer region and is non-constant there. Dashed curve for  $u$  denotes the inner asymptotic solution (8) with  $\xi$  determined by solving (30) (31), (32) simultaneously. Dashed curve for  $v$  shows the corresponding outer solution (30).

Type I solution satisfies  $u \sim 0$  in the outer region. Then  $v$  satisfies in the outer region,

$$v'' - v = 0, \quad x \gg \varepsilon, \quad v'(L) = 0$$

with the solution given by

$$v = A \cosh(x - L), \quad x \gg \varepsilon. \quad (9)$$

To determine the constant  $A$ , we match (9) to (8). We take the limit  $y \gg 1$  in (8) to obtain

$$\frac{d}{dy}v \sim -\varepsilon\sqrt{2\xi a}, \quad y \gg 1. \quad (10)$$

On the other hand for small  $x$  we have from (9),  $\frac{d}{dy}v = \varepsilon\frac{d}{dx}v \sim -\varepsilon A \sinh(L)$  for  $x \rightarrow 0$ . Matching with (10) yields

$$A = \frac{\sqrt{2\xi a}}{\sinh(L)}$$

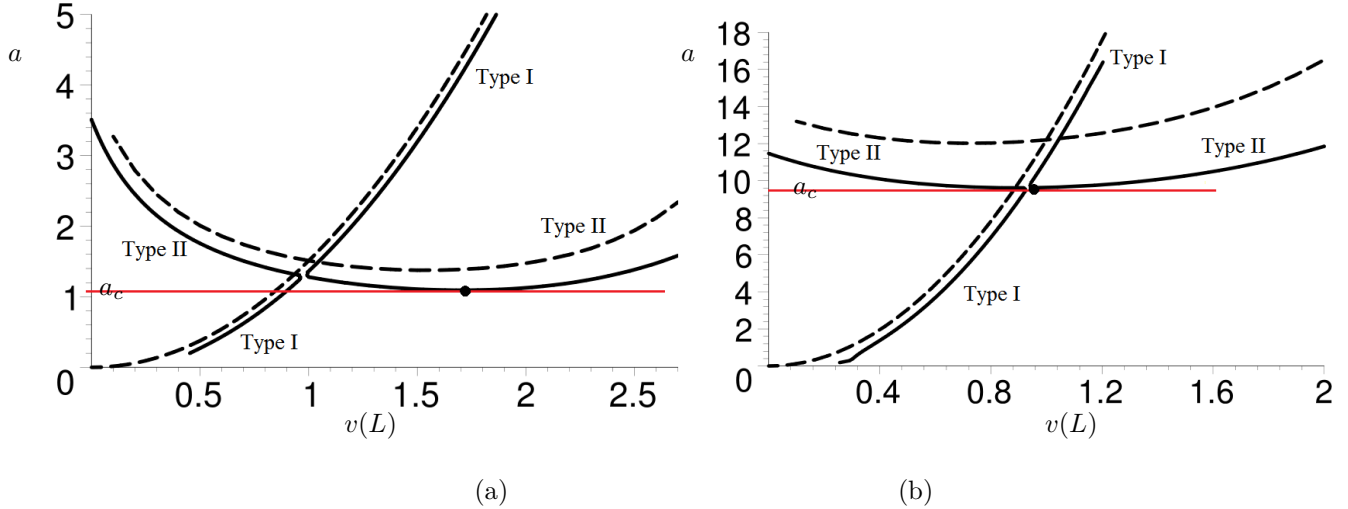


Figure 3: Bifurcation diagram for type I and II solutions. Solid curves denote the full problem whereas dotted curves are the asymptotics. The horizontal red line corresponds to the fold point  $a_c$ . (a)  $\varepsilon = 0.05$ ,  $L = 1.5$ . (b)  $\varepsilon = 0.15$ ,  $L = 2.5$ . Maple's boundary value problem solver and its continuation capabilities were used to compute the solid curves

so that

$$v_0 = \sqrt{2\xi a} \frac{\cosh(L)}{\sinh(L)}; \quad (11)$$

$$v = \sqrt{2\xi a} \frac{\cosh(x-L)}{\sinh(L)}, \quad x \gg \varepsilon. \quad (12)$$

Near the core of the spike,  $v$  has a corner layer in order to satisfy the condition  $v'(0) = 0$ . Indeed, from (8) we obtain

$$W_0 = -2 \ln \cosh \left( y \sqrt{\xi a / 2} \right)$$

so that in the inner region we obtain

$$v \sim v_0 - 2\varepsilon \ln \cosh \left( y \sqrt{\xi a / 2} \right).$$

The composite solution for  $v$  is then obtained using Van Dyke's matching principle [34, 35], that is,  $v_{unif} = v_{inner} + v_{outer} - v_{overlap}$ ; this yields

$$v \sim \frac{\sqrt{2\xi a}}{\sinh(L)} (\cosh(x-L) + \sinh(L)x) - 2\varepsilon \ln \left[ 2 \cosh \left( \frac{x}{\varepsilon} \sqrt{\xi a / 2} \right) \right]$$

It remains to determine the height  $\xi$ . To do so, we integrate the first equation in (5) to obtain the solvability condition  $\int_0^L (u - u^2) dx = 0$ . We then substitute (8) for  $u$ ; this yields, to leading order,

$$\xi = \frac{\int_0^\infty \operatorname{sech}^2(z) dz}{\int_0^\infty \operatorname{sech}^4(z) dz} = \frac{3}{2} \quad (13)$$

where we used the identities  $\int_0^\infty \operatorname{sech}^2(z) dz = 1$ ,  $\int_0^\infty \operatorname{sech}^4(z) dz = \frac{2}{3}$ . In summary, the uniform asymptotic expansion of type I equilibrium state of (5) is given by

$$u \sim \frac{3}{2} \operatorname{sech}^2 \left( \frac{x}{\varepsilon} \sqrt{\frac{3a}{4}} \right); \quad (14)$$

$$v = \frac{\sqrt{3a}}{\sinh(L)} (\cosh(x-L) + \sinh(L)x) - 2\varepsilon \ln \left[ 2 \cosh \left( \frac{x}{\varepsilon} \sqrt{3a/4} \right) \right]. \quad (15)$$

## 2.2 Stability analysis of Type I solution

We now proceed to study the stability of type I solutions. The analysis presented below builds on ideas from [19, 36].

Linearizing about the steady state, we write

$$u(x, t) = u(x) + e^{\lambda t} \phi(x); \quad v(x, t) = v(x) + e^{\lambda t} \psi(x), \quad \phi, \psi \ll 1$$

where we use  $u(x, t)$ ,  $v(x, t)$  to denote the full solution to (2) and  $u(x)$ ,  $v(x)$  to denote the symmetric spike equilibrium on domain  $[-L, L]$  as constructed in §2.1. For the rest of this section, we will use  $u$  to denote the equilibrium  $u(x)$  and similarly for  $v$ . The linearized equations are

$$\lambda \phi = \varepsilon \phi'' - (u\psi' + \phi v')' + (1 - 2u)\phi \quad (16)$$

$$\lambda \tau \psi = \psi'' + \frac{a}{\varepsilon} \phi - \psi. \quad (17)$$

The solution space of (16, 17) is split into two subspaces, depending on whether the eigenfunction is odd or even. These correspond to the following boundary conditions:

$$\textbf{Odd eigenfunction:} \quad \phi(0) = 0 = \psi(0); \quad \phi'(L) = 0 = \psi'(L) \quad (18)$$

$$\textbf{Even eigenfunction:} \quad \phi'(0) = 0 = \psi'(0); \quad \phi(L) = 0 = \psi(L) \quad (19)$$

We shall refer to the eigenvalue associated to odd (resp. even) eigenfunction as *odd* (resp. *even*) *eigenvalue*. In the inner region near the spike, we rescale as follows

$$x = \varepsilon y; \quad \phi(x) = \Phi(y); \quad \Psi = \Psi_0 + \varepsilon P(y);$$

Note that  $\Psi_0$  is a constant since to leading order  $\Psi$  satisfies  $\Psi_{yy} = 0$ . We then obtain the following exact equations for  $\Phi$  and  $P$ ,

$$\begin{aligned} \varepsilon \lambda \Phi &= \Phi_{yy} - (UP_y + \Phi W_y)_y + \varepsilon(1 - 2U)\Phi \\ \varepsilon \tau \lambda P &= P_{yy} + a\Phi + (\Psi_0 + \varepsilon P)\varepsilon. \end{aligned}$$

Expand in the power series in  $\varepsilon$  as

$$\lambda = \lambda_0 + \varepsilon \lambda_1 \dots; \quad \Phi = \Phi_0 + \varepsilon \Phi_1 + \dots; \quad P = P_0 + \varepsilon P_1 + \dots \quad (20)$$

so that to leading order we get

$$U_0 P_{0y} + \Phi_0 W_{0y} = 0; \quad P_{0yy} + a\Phi_0 = 0. \quad (21)$$

There are two linearly independent solutions to (21) which correspond to even (i.e. Dirichlet) or odd (i.e. Neumann) boundary conditions at the origin. The even solution to (21) corresponds to the scaling invariance of the inner problem (6) and is given by

$$\Phi_0 = \frac{\partial U_0}{\partial \xi}; \quad P_0 = \frac{\partial W_0}{\partial \xi}$$

where  $U_0$  and  $W_0$  are defined in (8). The odd solution to (21) corresponds to the translational invariance and is given by

$$\Phi_0 = U_{0y}; \quad P_0 = W_{0y}. \quad (22)$$

The eigenvalue is then determined by formulating an appropriate solvability condition.

**Even eigenvalue:** integrate (16) on  $[0, L]$ ; because of boundary conditions (18) we then obtain.

$$\lambda \int_0^L \phi dx = \int_0^L (1 - 2u) \phi dx. \quad (23)$$

Assume that  $\phi$  is exponentially small in the outer region; then the leading order to (23) becomes

$$\lambda_0 \int_0^\infty \frac{\partial U_0}{\partial \xi} dy = \int_0^\infty (1 - 2U_0) \frac{\partial U_0}{\partial \xi} dy.$$

Evaluating the integrals using (8) finally yields  $\lambda \sim -2$  so that the even eigenvalue is stable.

**Odd eigenvalue:** The odd solution to (21) is given by (22). To determine  $\lambda$ , multiply (16) by  $x$  and integrate. to obtain

$$\lambda \int_0^L x \phi dx = \int_0^L (u\psi' + \phi v') dx + \int_0^L (1 - 2u) \phi x dx. \quad (24)$$

To estimate  $\int_0^L (u\psi' + \phi v') dx$ , multiply (17) by  $v_x$  and integrate by parts. First note that

$$\begin{aligned} \int_0^L \psi'' v' dx &= -\psi(L)v''(L) + \int_0^L \psi v''' dx \\ &= -\psi(L)v''(L) + \int_0^L \psi v' dx + \frac{a}{\varepsilon} \int_0^L \psi' u dx \end{aligned}$$

so that

$$\begin{aligned} \tau \lambda \int_0^L \psi v' dx &= -\psi(L)v''(L) + \frac{a}{\varepsilon} \int_0^L (\psi' u + v' \phi) dx; \\ \int_0^L (\psi' u + v' \phi) dx &= \frac{\varepsilon \tau \lambda}{a} \int_0^L \psi v' dx + \frac{\varepsilon}{a} \psi(L)v''(L). \end{aligned} \quad (25)$$

We therefore obtain an *exact expression*

$$\lambda \int_0^L x \phi dx = \frac{\varepsilon}{a} \psi(L)v''(L) + \frac{\varepsilon \tau \lambda}{a} \int_0^L \psi v' dx - \int_0^L (1 - 2u) \phi x dx. \quad (26)$$

Next we estimate

$$\int_0^L x \phi dx \sim \varepsilon^2 \int_0^\infty y U_{0y} dy = -\varepsilon^2 \int_0^\infty U_0 dy = -\varepsilon^2 \sqrt{2\xi/a} \quad (27)$$

and

$$\int_0^L (1 - 2u) \phi x dx \sim \varepsilon^2 \int_0^\infty (1 - 2U_0) U_{0y} y dy = -\varepsilon^2 \int_0^\infty (U_0 - U_0^2) dy = 0. \quad (28)$$

so that (26) becomes

$$\varepsilon \sqrt{2\xi a} \lambda = -\psi(L)v''(L) - \tau \lambda \int_0^L \psi v' dx.$$

We recall from (12) that  $v(x) \sim \frac{\sqrt{2a\xi}}{\sinh(L)} \cosh(L - x)$  so that

$$v''(L) = \frac{\sqrt{2a\xi}}{\sinh(L)}.$$

It remains to determine  $\psi$ . For concreteness, consider at first the case  $\tau = 0$ . Then  $\psi$  satisfies

$$\psi'' - \psi \sim -\frac{a}{\varepsilon} U_{0y} \sim A \delta'(x)$$

where

$$A = \int_0^L x \frac{a}{\varepsilon} U_{0y} dx \sim \varepsilon a 2 \int_0^\infty y U_{0y} dy = -2\varepsilon \sqrt{2\xi a}.$$

It follows that

$$\psi(x) = -\varepsilon \sqrt{2a\xi} \frac{\cosh(L - x)}{\cosh L}$$

so that

$$\lambda = \frac{\sqrt{2\xi a}}{\sinh L \cosh L}; \quad \tau = 0.$$

This shows that in the case  $\tau = 0$ , the odd eigenvalue is unstable. More generally for an arbitrary  $\tau$ , an analogous computation yields the following equation for  $\lambda$ ,

$$\lambda \frac{\sinh L \cosh(\mu L)}{\sqrt{2\xi a}} = \cosh L \cosh \mu L - \mu \sinh \mu L \sinh L; \quad \mu = \sqrt{1 + \lambda \tau}. \quad (29)$$

We claim that (29) has a solution with  $\lambda > 0$ . Indeed,  $lhs(29) \rightarrow \infty$  as  $\lambda \rightarrow \infty$  and  $rhs(29) \rightarrow -\infty$  as  $\lambda \rightarrow \infty$ . On the other hand, when  $\lambda = 0$  we have  $lhs(29) = 0$  and  $rhs(29) = 1$ . Thus by intermediate value theorem there is a positive (i.e. unstable) eigenvalue. We summarize our results as follows.

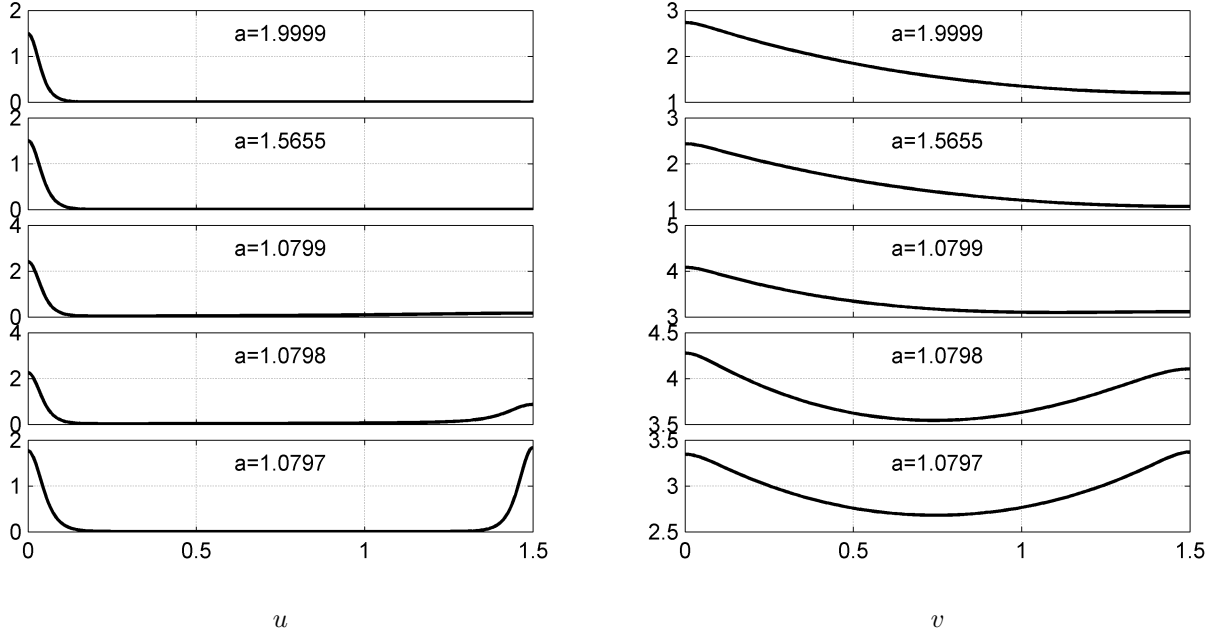


Figure 4: Evolution of (2) with  $\varepsilon = 0.05$ ,  $L = 1.5$  and  $a = 2 - 10^{-4}t$ . Due to the fold point bifurcation, spike insertion occurs as  $a$  is decreased below  $a_c \sim 1.08$ . FlexPDE [31] was used for numerical computations

**Theorem 2.1** *A symmetric spike of Type 1 centered at the origin on the domain  $[-L, L]$  is stable with respect to even eigenvalue but is unstable with respect to odd (translational) eigenvalue for all  $\tau > 0$ .*

The stability of an even eigenfunction is sometimes referred to as *structural stability*: it means that even though the spike is translationally unstable, it does not disappear but simply moves away from its central location and towards the boundary. This dynamical behaviour is qualitatively illustrated in Figure 5(a). On the other hand, a spike at the boundary, or a half-spike centered at 0 on the domain  $[0, L]$ , does not admit translational mode (19), and only admits the even mode (18). As a corollary of Theorem 2.1, a single boundary spike is *stable*. This is also seen numerically in Figure 5(a): after the spike merges with the boundary, it remains there as a stable steady state.

### 3 Type II solutions

Type II solutions co-exist with type I solutions constructed in the previous section, in the regime given by equations (2), whose steady state equations are given by (5). The spike construction in the *inner* region  $|x| \leq O(\varepsilon)$  is identical to the equations (8). The difference is that in the *outer* region,  $u$  is no longer assumed to be zero. Then the height  $\xi$  in (8) will longer given by  $3/2$  but rather will be determined along with the outer solution for  $u$  and  $v$ . Away from the spike in the outer region  $|x| \gg O(\varepsilon)$  we rescale

$$u = \varepsilon \hat{u}.$$

Then to leading order the steady state satisfies

$$(\hat{u}v_x)_x = \hat{u}; \quad v_{xx} - v + \hat{u}a = 0.$$

Solving for  $\hat{u} = \frac{v-v''}{a}$  we then obtain a third-order ODE for  $v$  in the outer region,

$$(v - v'')(v'' - 1) + (v - v'')'v' = 0. \tag{30}$$

Since  $v'(L) = 0$ , either  $v''(L) = 1$  or else  $\hat{u}(L) = 0$ . The latter corresponds to Type I solutions so here we assume that  $v''(L) = 1$ . We then solve (30) subject to the boundary conditions

$$v(L) = A; \quad v'(L) = 0; \quad v''(L) = 1 \tag{31}$$

where the constant  $A$  and  $\xi$  are to be found.

To match the outer and inner region, integrate the second equation in (5) on a small interval  $[0, \delta]$  where  $\varepsilon \ll \delta \ll 1$ . This yields

$$v_x(\delta) + \frac{a}{\varepsilon} \int_0^\delta u dx = \int_0^\delta v dx$$

We further estimate

$$\frac{a}{\varepsilon} \int_0^\delta u dx = a \int_0^{\delta/\varepsilon} U(y) dy \sim \int_0^\infty a U_0 dy = \sqrt{2\xi a}$$

and

$$\int_0^\delta v dx = O(\delta).$$

Therefore to leading order in the outer region we obtain

$$v'(0^+) = -\sqrt{2\xi a}.$$

Similarly integrating the first equation in (5) yields an additional equation

$$\int_0^\infty (U_0 - U_0^2) dy + \int_0^L \hat{u}(x) dx \sim 0.$$

Using the identities  $\int_0^\infty \operatorname{sech}^2(s) ds = 1$ ,  $\int_0^\infty \operatorname{sech}^4(s) ds = \frac{2}{3}$  we obtain

$$\int_0^\infty (U_0 - U_0^2) dy = \xi \left(1 - \frac{2}{3}\xi\right) \sqrt{\frac{2}{\xi a}}.$$

We also evaluate

$$\begin{aligned} \int_0^L \hat{u}(x) dx &= \int_0^L (\hat{u}v')' dx = -\hat{u}(0)v'(0) \\ &= \hat{u}(0)\sqrt{2\xi a} \end{aligned}$$

so that

$$1 - \frac{2}{3}\xi = -\hat{u}(0)a; \quad v'(0) = -\sqrt{2\xi a}; \quad \hat{u}(0) = \frac{v(0) - v''(0)}{a}.$$

Solving for  $a$  and  $\xi$  yields

$$a = \frac{v'(0)^2}{3(1 + v(0) - v''(0))}; \quad \xi = \frac{3}{2}(1 + v(0) - v''(0)). \quad (32)$$

Note that  $v(0)$ ,  $v'(0)$  and  $v''(0)$  are can be viewed as a function of the parameter  $A = v(L)$ . Thus (32) together with (30, 31) defines a parametric curve  $a(L), \xi(L)$  in the  $a, \xi$  plane. Figure 3 shows the graph of  $a$  as a function of  $A = v(L)$ . There are two such curves, one for type I and another for type II solutions. In the asymptotic limit  $\varepsilon \rightarrow 0$  (shown by dashed curves) these curves intersect near  $A = 1$ . For small but positive  $\varepsilon$ , the two branches connect to each-other near  $A = 1$  (solid curves). Thus the branch to the left of  $A \sim 1$  is such that  $u(L) < 0$ ; this follows from the fact that the outer solution satisfies  $\hat{u} = \frac{v-v''}{a}$  with  $v''(L) \sim 1$ . Similarly, the branch to the right of  $A = 1$  has  $u, v > 0$ .

As Figure 3 shows, the bifurcation curves of type I and type II intersect at  $A = 1$  in the asymptotic limit  $\varepsilon \rightarrow 0$ . For any positive value of  $\varepsilon$ , the two curves cannot cross due to uniqueness of the solution; instead they fold over. When  $L = 2.5$ , the fold point occurs near  $A \sim 1$ . On the other hand, when  $L = 1.5$ , the bifurcation curve has a fold point around  $A \sim 1.7 > 1$ , as shown in the figure. So there is some critical value of  $L = L^*$  for which the bifurcation structure changes. This critical value occurs precisely when the asymptotics of the type II curve (indicated by dashed line the figure) has a horizontal tangent at  $A = 1$ . Fortunately, the asymptotics near  $A \sim 1$  can be explicitly computed as we now show.

**Asymptotics near  $A \sim 1$ .** We set

$$A = 1 + \delta; \quad \delta \ll 1.$$

For simplicity, we also change variables

$$z = L - x.$$

When  $\delta = 0$ , the solution to (30, 31) is given by  $v = \cosh(z)$ . More generally, for small  $\delta$  we expand

$$v = \cosh(z) + v_1(z)\delta. \quad (33)$$

We then obtain the ODE

$$\frac{d}{dz} \ln(v_1 - v_1'') = \frac{1 - \cosh z}{\sinh z}$$

along with the boundary conditions

$$v_1(0) = 1; \quad v_1'(0) = 0; \quad v_1''(0) = 0.$$

We note that

$$\int \frac{1 - \cosh z}{\sinh z} dz = \ln(\operatorname{sech}^2(z/2)) + C$$

so that

$$v_1'' - v_1 = K \operatorname{sech}^2(z/2)$$

where  $K$  is some constant. Substituting in the initial conditions we obtain

$$v_1'' - v_1 = -\operatorname{sech}^2(z/2); \quad v_1(0) = 1; \quad v_1'(0) = 0.$$

Next we substitute (33) into (32) to obtain

$$3a = \sinh^2 L + \delta (2v_1'(L) \sinh L - \sinh^2 L \operatorname{sech}^2(L/2)).$$

The expression for  $v_1'(L)$  is computed using the variation of parameters as follows

$$v_1'(z) = \sinh(z) - \int_0^z \cosh(z-s) \operatorname{sech}^2(s/2) ds. \quad (34)$$

We have  $\frac{da}{dA}|_{A=1} = 0$  if and only if

$$2v_1'(L) = \sinh L \operatorname{sech}^2(L/2). \quad (35)$$

It is easy to show that (35) has a root; in fact its uniqueness can also be shown using convexity arguments. Using Maple to evaluate the integral in (34), we find that the unique root of (35) is given by

$$L^* = 2.202162338. \quad (36)$$

It follows that  $\frac{da}{dA}|_{A=1}$  is positive when  $L > L^*$  and is negative when  $L < L^*$ .

Note that at the intersection point  $A = 1$ , we have  $a = \frac{1}{3} \sinh^2(L)$ . Now consider the case  $L > L^*$ . In this case, numerical computations of the limiting problem (30, 31, 32) show that  $a(A)$  is an increasing function of  $A$  for  $A > 1$  (dashed curve in Figure 3(b)). On the other hand, the bifurcation curves corresponding to type I and type II solutions cannot cross each other due to uniqueness of solutions to ODE's. Numerically, their connection is observed as shown in Figure 3. In the case  $L < L^*$ , this connection implies the existence of the fold point near  $A = 1$ ,  $a_c \sim \frac{1}{3} \sinh^2(L)$ . More generally, we now show that  $a \rightarrow \infty$  as  $A \rightarrow \infty$ , confirming the existence of the fold point.

**Large  $A$  limit:** in this case we rescale  $v = A\hat{v}$  so that (30) becomes

$$(\hat{v} - \hat{v}'') \left( \hat{v}'' - \frac{1}{A} \right) + (\hat{v} - \hat{v}'')' \hat{v}' = 0;$$

subject to boundary conditions

$$\hat{v}(L) = 1; \quad \hat{v}'(L) = 0; \quad \hat{v}''(L) = 1/A.$$

To leading order, we obtain:

$$\ln(\hat{v} - \hat{v}'') + \ln \hat{v}' = O(1/A)$$

so that

$$(\hat{v} - \hat{v}'') \hat{v}' \sim 0.$$

Therefore

$$v \sim A \cosh(x - L)$$

from where we determine the asymptotics

$$a \sim \frac{A^2 \sin^2 L}{3}; \quad A \gg 1.$$

This shows that  $a \rightarrow \infty$  as  $A \rightarrow \infty$ , in the asymptotic limit  $\varepsilon \rightarrow 0$ .

We summarize our finding as follows.

**Proposition 3.1** (*Type II solutions*) A type II solution to (5) is such  $u$  has a spike of  $O(1)$  at the center while in the outer region,  $u(x)/\varepsilon$  is  $O(1)$  and is non-zero for  $|x| \gg O(\varepsilon)$ . There exists a number  $a_c$  such that Type II solution exists if and only if  $a > a_c$ . If  $L < L^* = 2.20216$  then  $a_c < \frac{1}{3} \sin^2 L$ . If  $L \geq L^*$  then  $a_c \sim \frac{1}{3} \sin^2 L$ . The solution disappears at the fold point bifurcation as  $a$  is decreased below  $a_c$ .

The number  $a_c$  corresponds to the fold point, and is responsible for spike insertion. To illustrate this, consider Figure 4. We take  $L = 1.5$  and consider initial solution in the form of a single spike of type I at the left boundary. Initially, we take  $a = 2$  and then slowly increase  $a$  in time according to the formula  $a = 2 - 10^{-4}t$ . As shown in the figure, a new spike rises out of the background state at around  $a \approx 1.08$ , which corresponds to the critical value  $a_c$  at the fold point, as seen from Figure 3(a).

## 4 Type III solutions

So far, we have described two regimes for both of which the interior spike is translationally unstable: we have shown this for type I solutions in section 2. While we did not perform the stability analysis for type II solutions, the numerical simulations we performed indicate that type II solutions discussed in section 3 are indeed unstable and move towards the boundary. This raises the question, *is there a regime for which an interior spike is stable?* The goal of this section is to answer this question in the affirmative. Namely, we consider the following rescaling of the equations (1)<sup>2</sup>,

$$u_t = u_{xx} - (uv_x)_x + u - u^2, \quad \tau v_t = \varepsilon^2 v_{xx} - a\varepsilon v + u, \quad x \in [-L, L] \quad (37)$$

where we additionally assume that  $0 < \varepsilon \ll 1$  and  $a, L$  are positive  $O(1)$  parameters. Biologically, this corresponds to small diffusion of chemo-attractant (relative to cell diffusion or chemotaxis-induced motion), and slow chemo-attractant decay rate (relative to chemo-attractant production by the cells).

First, consider the steady state equations

$$0 = u_{xx} - (uv_x)_x + u - u^2, \quad 0 = \varepsilon^2 v_{xx} - a\varepsilon v + u. \quad (38)$$

As before, we start by constructing a half-spike on domain  $[0, L]$  with Neumann boundary conditions for  $u, v$  at  $x = 0, L$ ; the interior spike is then obtain by even reflection through the origin. It turns out that the steady state for  $U$  has three distinct layers which we will refer to as the inner, middle and outer layers, and which scale as follows:

$$\begin{aligned} \text{Inner layer: } & x = \varepsilon y \quad u(x) = U(y) \\ \text{Middle layer: } & x = (\varepsilon/a)^{1/2} z, \quad u(x) = \mathcal{U}(z) \\ \text{Outer layer: } & x = x \end{aligned}$$

We now go through the construction inside each layer and their matchings.

*Inner layer:* To leading order, the equations in the inner layer are the same as for Type I, namely,

$$V_{yy} + U = 0; \quad U_{yy} - (UV_y)_y \sim 0. \quad (39)$$

As before, we obtain

$$U = \xi \operatorname{sech}^2(\sqrt{\xi/2}y); \quad V = \ln(U) + C \quad (40)$$

where the constants  $\xi$  and  $C$  will be determined through matching later.

The constant  $\xi$  is determined by integrating the first equation in (37) on  $[0, L]$ . Similarly to type I solution, it will be shown below that the contributions of the middle and outer regions are negligible. Similarly to section 2.1 we then obtain that  $\xi = 3/2$ .

<sup>2</sup>Equations (37) are obtained from (1) via the following transformations, after dropping the \*'s:

$$\begin{aligned} x &= \sqrt{\frac{D_u}{r}} x^*, \quad v = \frac{D_u}{\chi} v^*, \quad u = K u^*, \quad t = \frac{1}{r} t^* \\ \varepsilon &= \sqrt{\frac{D_v}{D_u}}, \quad a = \frac{\alpha K}{\beta \sqrt{D_u D_v}}, \quad \tau = r/\beta. \end{aligned}$$

*Middle layer:* to leading order, we have

$$\mathcal{V}_{zz} - \mathcal{V} = \frac{\mathcal{U}}{a\varepsilon} \quad \mathcal{U}_{zz} + (\mathcal{U}\mathcal{V}_z)_z \sim 0 \quad (41)$$

Moreover, we make a self-consistent ansatz that  $\frac{\mathcal{U}}{\alpha_0\varepsilon} \ll O(\mathcal{V})$  in the middle region; this consistency condition will be validated below by matching the inner and middle layer. Since  $V$  must remain bounded for  $z \gg 1$ , we then obtain

$$\mathcal{V} \sim Ae^{-z}. \quad (42)$$

We now match the inner and the middle layer. Expanding (40) for large  $y$  we obtain

$$\begin{aligned} U &\sim 4\xi \exp(-\sqrt{2\xi}y), \quad y \gg 1; \\ V &\sim \ln(4\xi) + C - \sqrt{2\xi}y, \quad y \gg 1. \end{aligned} \quad (43)$$

On the other hand, expanding (42) for small  $z = \varepsilon^{1/2}a^{1/2}y$  we obtain

$$\mathcal{V} \sim A(1 - \varepsilon^{1/2}a^{1/2}y) \quad (44)$$

Matching (43) and (44) inbetween inner and middle layer  $1 \ll y \ll O(\varepsilon^{-1/2})$  yields

$$A = \sqrt{\frac{2\xi}{a\varepsilon}}; \quad C = A - \ln(4\xi).$$

Since the equation for  $\mathcal{U}$  in (41), is the same as (39), we obtain that (40) also holds with  $U, V$  replaced by  $\mathcal{U}, \mathcal{V}$ . Thus we obtain

$$V = \ln U - \ln 4\xi + A$$

so that

$$\begin{aligned} U &\sim 4\xi \exp(Ae^{-z} - A) \\ &\sim 4\xi \exp(-A), \quad z \gg 1. \end{aligned} \quad (45)$$

*Outer layer:* Since  $\mathcal{U}$  and  $\mathcal{V}$  are both small for  $z \gg 1$ , the dominant terms in (38) in the outer region become

$$u_{xx} + u = 0, \quad x \gg O((\varepsilon/a)^{1/2}).$$

Imposing the boundary condition  $u_x(L) = 0$  we then obtain

$$u \sim B \cos(x - L), \quad x \gg O(\varepsilon^{1/2}).$$

Matching to the middle layer (45) we then obtain

$$B = \frac{4\xi}{\cos L} \exp(-A) = \frac{4\xi}{\cos L} \exp\left(-\sqrt{\frac{2\xi}{a\varepsilon}}\right). \quad (46)$$

The equation for  $v$  then becomes

$$\varepsilon^2 v'' - a\varepsilon v + B \cos(x - L) \sim 0.$$

Recalling that  $v'(L) = 0$ , its solution is given by

$$v \sim \frac{B}{a\varepsilon} \cos(x - L) + D \left\{ \exp\left((x - L)\sqrt{\frac{a}{\varepsilon}}\right) + \exp\left((L - x)\sqrt{\frac{a}{\varepsilon}}\right) \right\}$$

Matching to the inner layer, we get

$$D = A \exp\left(-L\sqrt{\frac{a}{\varepsilon}}\right) = \sqrt{\frac{2\xi}{a\varepsilon}} \exp\left(-L\sqrt{\frac{a}{\varepsilon}}\right).$$

We summarize this construction as follows.

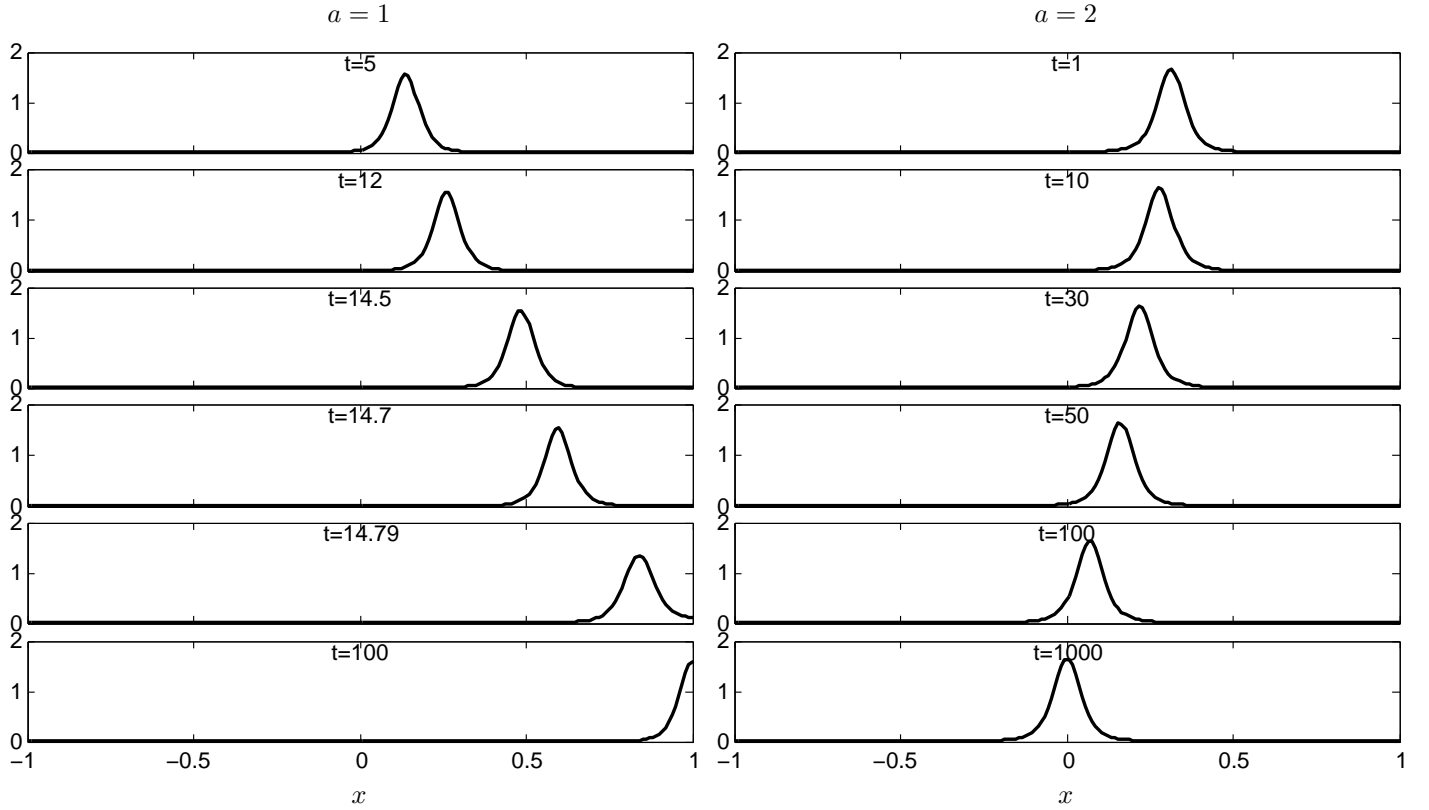


Figure 5: Numerical simulation of (37) with  $\varepsilon = 0.05$ ,  $\tau = 1$ . Left:  $a = 1$ , the interior spike is unstable and moves to the boundary. Right:  $a = 2$ , the interior spike is stable. FlexPDE [31] was used for numerical computations.

**Proposition 4.1** (type III steady state) *Suppose that  $0 < L < \pi/2$ . Then the steady state to (38) on domain  $[-L, L]$  with Neumann boundary conditions which has even symmetry with respect to the origin is given by*

$$\begin{aligned}
 u(x) &\sim \begin{cases} \frac{3}{2} \operatorname{sech}^2(\sqrt{3}x/(2\varepsilon)), & |x| \leq O(\varepsilon) \\ 6 \exp\left(\sqrt{\frac{3}{a\varepsilon}}[\exp(-|x|/\sqrt{\varepsilon}) - 1]\right), & O(\varepsilon) \ll |x| \leq O(\sqrt{\varepsilon}) \\ \frac{6 \exp(-\sqrt{\frac{3}{a\varepsilon}})}{\cos L} \cos(|x| - L), & O(\sqrt{\varepsilon}) \ll |x| \leq L \end{cases} \\
 v(x) &\sim \begin{cases} \ln(u) - \ln 6 + \sqrt{\frac{6}{a\varepsilon}}, & |x| \leq O(\sqrt{\varepsilon}) \\ \frac{6 \exp(-\sqrt{\frac{3}{a\varepsilon}})}{a\varepsilon \cos L} \cos(|x| - L) + \sqrt{\frac{6}{a\varepsilon}} \exp(-L\sqrt{\frac{a}{\varepsilon}}) 2 \cosh((|x| - L)\sqrt{\frac{a}{\varepsilon}}), & O(\sqrt{\varepsilon}) \ll |x| \leq L \end{cases}
 \end{aligned}$$

Note that in the outer region  $|x| \gg O(\sqrt{\varepsilon})$ , the solution for  $u$  is exponentially small in  $\varepsilon$ ; however unlike the type I solution, it does not decay exponentially, and is actually increasing in that region. Also, the outer solution for  $v$  consists of two competing terms; in particular we have

$$v(L) \sim \frac{6}{\varepsilon a \cos L} \exp\left(-\sqrt{\frac{3}{a\varepsilon}}\right) + \sqrt{\frac{6}{a\varepsilon}} 2 \exp\left(-L\sqrt{\frac{a}{\varepsilon}}\right). \quad (47)$$

The stability of the small eigenvalue is precisely determined by which of the two terms in (47) is dominant. We now state the main result of this section.

**Theorem 4.2** *Consider the steady state as constructed in Proposition 4.1 to the system (37) on  $[-L, L]$  with Neumann boundary conditions. Suppose that  $\tau = 0$ . In the limit  $\varepsilon \rightarrow 0$ , this steady state is stable if  $L > \sqrt{3}/a$  and is unstable if  $L < \sqrt{3}/a$ . The instability is due to the odd eigenfunction.*

The eigenvalue problem associated with (37) corresponding to the odd eigenfunction with  $\tau = 0$  is

$$\lambda\phi = \phi'' - (u\psi' + \phi v')' + \phi - 2u\phi; \quad (48)$$

$$0 = \psi'' - \frac{a}{\varepsilon}\psi + \frac{1}{\varepsilon^2}\phi; \quad (49)$$

$$\phi(0) = 0 = \psi(0); \quad \phi_x(L) = 0 = \psi_x(L). \quad (50)$$

where  $u, v$  is the steady state to (37). Retracing the derivation of (24) leads to the following identity:

$$\lambda \int_0^L x\phi dx = -\phi(L) + a\varepsilon\psi(L)v(L) + \int_0^L x(1-2u)\phi dx. \quad (51)$$

In the inner and middle region, we estimate that  $(\phi, \psi) = (u', v')$ . This solution satisfies equations (48, 49) as well as the Dirichlet boundary conditions at 0. However it does not satisfy the Neumann boundary condition at  $L$ , so the outer region must be considered separately. Assuming that  $\lambda \ll 1$ , the solution in the outer region satisfies to leading order

$$\phi'' + \phi \sim 0, \quad x \gg O(\sqrt{\varepsilon})$$

so that

$$\phi \sim \hat{B} \cos(x - L), \quad x \gg O(\sqrt{\varepsilon}).$$

To determine the constant  $\hat{B}$ , we match with the intermediate region  $\phi \sim u'$ . In the regime  $O(\sqrt{\varepsilon}) \ll x \ll 1$  we have

$$\begin{aligned} u &\sim B \cos(x - L) \\ &\sim B \cos(L) + Bx \sin(L) + O(x^2) \end{aligned}$$

where  $B$  is given by (46). Then  $u_x \sim B \sin(L) \sim \hat{B} \cos(L)$  so that

$$\hat{B} = B \tan(L) = \phi(L).$$

The equation for  $\psi$  then becomes

$$\psi'' - a/\varepsilon\psi + \hat{B} \cos(x - L) \sim 0$$

so that

$$\psi \sim \frac{1}{a\varepsilon} \hat{B} \cos(x - L) + \hat{A} \left\{ \exp\left((x - L)\sqrt{\frac{a}{\varepsilon}}\right) + \exp\left((L - x)\sqrt{\frac{a}{\varepsilon}}\right) \right\}$$

The constant  $\hat{A}$  is determined by matching the outer region to the inner region where

$$v_x \sim -\frac{\sqrt{2\xi a}}{\varepsilon} \exp\left(-x\sqrt{\frac{a}{\varepsilon}}\right), \quad O(\sqrt{\varepsilon}) \leq x \ll O(1)$$

so that

$$\hat{A} = -\frac{\sqrt{2\xi a}}{\varepsilon} \exp\left(-L\sqrt{\frac{a}{\varepsilon}}\right).$$

This yields

$$\psi(L) \sim \frac{1}{a\varepsilon} \frac{4\xi \tan L}{\cos L} \exp\left(-\sqrt{\frac{2\xi}{a\varepsilon}}\right) - \frac{\sqrt{8\xi a}}{\varepsilon} \exp\left(-L\sqrt{\frac{a}{\varepsilon}}\right).$$

Next we compute the integral term on the right hand side of (51). Let  $\delta$  be any number with  $\sqrt{\varepsilon} \ll \delta \ll 1$  and split

$$\int_0^L x\phi(1-2u) dx = \int_0^\delta + \int_\delta^L = I_1 + I_2.$$

We compute

$$I_1 \sim \int_0^\delta x u_x (1-2u) dx \sim - \int_0^\delta (U - U^2) dx.$$

We then use the fact that

$$0 = \int_0^L (u - u^2) dx = \int_0^\delta (U - U^2) dx + \int_\delta^L B \cos(x - L) dx$$

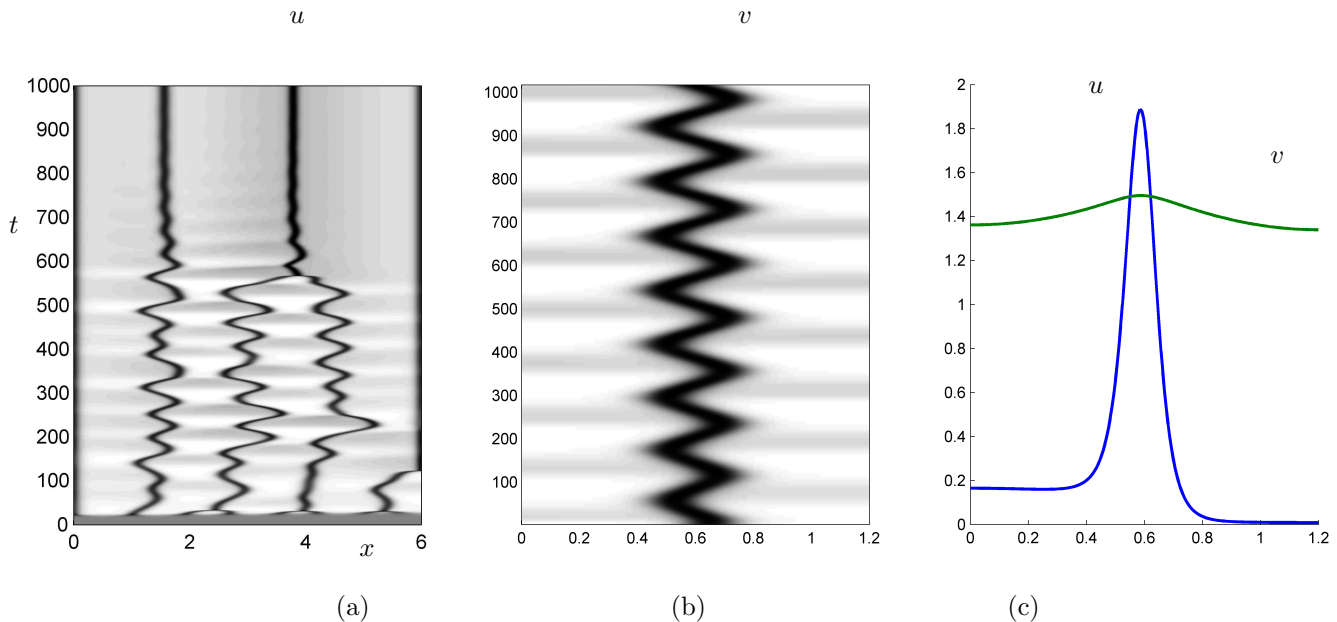


Figure 6: Oscillatory dynamics in the system (2). (a)  $\tau = 50, \varepsilon = 0.02, a = 0.075$ . (b)  $\tau = 200, \varepsilon = 0.3, a = 0.075$ . (c) The snapshot of the solution at the final time  $t = 1018$  with parameters as in (b).

so that

$$I_1 \sim \int_0^L B \cos(x - L) dx \sim B \sin L.$$

For  $I_2$  we estimate

$$I_2 \sim \int_0^L x \hat{B} \cos(x - L) dx = \hat{B}(1 - \cos L) = \phi(L) - B \sin L$$

Thus we get  $\int_0^L x \phi(1 - 2u) dx = \phi(L)$  so that (51) becomes

$$\lambda \int_0^L x \phi dx = a \varepsilon \psi(L) v(L).$$

Finally we estimate

$$\int_0^L x \phi dx \sim - \int_0^\infty U dy < 0.$$

Since  $v(L) > 0$ , it follows that  $\lambda < 0$  provided that  $\psi(L) > 0$ ; otherwise  $\lambda \geq 0$  is unstable. To leading order the threshold  $\psi(L) = 0$  is achieved when  $L \sim L_c$  where

$$L_c = \sqrt{\frac{2\xi}{a}} \quad (52)$$

with  $\lambda \leq 0$  when  $L_c \leq L$ .

To conclude the proof of theorem 4.2, it suffices to show that the even eigenvalue is stable. The argument here is identical to the analysis of stability of the even eigenvalue for type I solutions as given in section 2.2. The key to that argument is the observation that  $u$  is exponentially small in the outer region, so that the integral  $\int_0^L u^p dx$  is well-approximated by assuming that  $u$  is negligible in the outer region. ■

## 5 Discussion

The chemotaxis model (1) introduced in [21] exhibits a surprising variety of spike dynamics. In this paper, we studied some of the mechanisms that drive these dynamics. We have identified three types of solutions. For type I solution, a single interior spike is unstable and moves towards the boundary of the domain. For type II solution, spike-insertion can

be observed. Stability thresholds are established for the type III solution. These mechanisms provide for basic building blocks from which more complex dynamics can be constructed.

The instability of type I solution is qualitatively similar to the behaviour of a spike for the classical KS model in one dimension. However there are no analogues for behaviours of type II and III solutions in the classical KS model. The production terms in (1) are essential for spike insertion and stabilization behaviours observed in type II and III solutions. To our knowledge, this is the first result showing analytically that an interior spike can be stable for Keller-Segel type models.

Spike solutions are commonplace in many other reaction-diffusion models. The stability theory for localized spikes was first developed for Gierer- Meinhardt model [37] and Gray-Scott model [38]. For both of these models, the basic question about the stability of a single spike with respect to the even eigenvalue reduces to the study of the so-called nonlocal eigenvalue problem (NLEP), which has terms that involve the integral of the eigenfunction itself [39]. For the KS model, the stabilization mechanism is completely different: due to a scaling invariance in the inner region, the even eigenvalue can be computed explicitly and no NLEP problem arises.

For simplicity, we only considered a single spike in this paper. The analysis of stability can be extended to multiple spikes using Floquet-type theory such as was done for example in [40, 41, 37]. Another open problem is to derive the equations of spike motion, such as was done for example in [37] for the Gierer-Meinhardt model.

Finally, there are other regimes of interest in this model. Numerical simulations from [28] show that the spikes can exhibit oscillations. Examples of these are shown in figure 6. It remains an open question to explain and quantify how these oscillations occur.

## Acknowledgments

We thank the anonymous referees for very useful comments, corrections and suggestions that have helped to improve the paper substantially. The research of the first author is supported by a grant from AARMS CRG in Dynamical Systems and NSERC grant 47050. He is also grateful for the hospitality of Juncheng Wei and CUHK, Mathematics department, where part of this paper was written. The research of the second author is partly supported by a General Research Fund from RGC of Hong Kong.

## References

- [1] E. Keller, L. Segel, Initiation of slime mold aggregation viewed as an instability, *Journal of Theoretical Biology* 26 (3) (1970) 399–415.
- [2] E. F. Keller, L. A. Segel, Model for chemotaxis, *Journal of Theoretical Biology* 30 (2) (1971) 225–234.
- [3] T. Hofer, J. A. Sherratt, P. K. Maini, Dictyostelium discoideum: cellular self-organization in an excitable biological medium, *Proceedings of the Royal Society of London. Series B: Biological Sciences* 259 (1356) (1995) 249–257.
- [4] J. J. Tyson, J. Murray, Cyclic amp waves during aggregation of dictyostelium amoebae, *Development* 106 (3) (1989) 421–426.
- [5] R. Tyson, S. Lubkin, J. Murray, A minimal mechanism for bacterial pattern formation, *Proceedings of the Royal Society of London. Series B: Biological Sciences* 266 (1416) (1999) 299–304.
- [6] D. Woodward, R. Tyson, M. Myerscough, J. Murray, E. Budrene, H. Berg, Spatio-temporal patterns generated by salmonella typhimurium, *Biophysical journal* 68 (5) (1995) 2181–2189.
- [7] P. Maini, M. Myerscough, K. Winters, J. Murray, Bifurcating spatially heterogeneous solutions in a chemotaxis model for biological pattern generation, *Bulletin of mathematical biology* 53 (5) (1991) 701–719.
- [8] J. Murray, M. Myerscough, Pigmentation pattern formation on snakes, *Journal of theoretical biology* 149 (3) (1991) 339–360.
- [9] M. R. Owen, J. A. Sherratt, Mathematical modelling of macrophage dynamics in tumours, *Mathematical Models and Methods in Applied Sciences* 9 (04) (1999) 513–539.

- [10] J. D. Murray, *Mathematical biology*, Vol. 2, springer, 2002.
- [11] T. Hillen, K. J. Painter, A users guide to pde models for chemotaxis, *Journal of mathematical biology* 58 (1-2) (2009) 183–217.
- [12] D. Horstmann, From 1970 until present: The keller-segel model in chemotaxis and its consequences i., *Jahresber. Deutsch. Math. -Verein.* 105 (3) (2003) 103–165.
- [13] S. Childress, J. Percus, Nonlinear aspects of chemotaxis, *Math Biosciences* 56 (1981) 217–237.
- [14] M. A. Herrero, J. J. L. Velázquez, Chemotactic collapse for the keller-segel model, *J. Math. Biol.* 35 (1996) 583–623.
- [15] W. Jager, S. Luckhaus, On explosions of solutions to a system of partial differential equations modelling chemotaxis, *Trans. Am. Math. Soc.* 329 (2) (1992) 819–824.
- [16] J. J. L. Velazquez, Point dynamics in a singular limit of the keller-segel model i: Motion of the concentration regions, *SIAM J. Appl. Math.* 64 (4) (2004) 1198–1223.
- [17] J. J. L. Velazquez, Point dynamics in a singular limit of the keller-segel model II: Formation of the concentration regions, *SIAM J. Appl. Math.* 64 (4) (2004) 1224–1248.
- [18] Y. Dolak, C. Schmeiser, The keller–segel model with logistic sensitivity function and small diffusivity, *SIAM Journal on Applied Mathematics* 66 (1) (2005) 286–308.
- [19] K. Kang, T. Kolokolnikov, M. Ward, The stability and dynamics of a spike in the 1d keller–segel model, *IMA journal of applied mathematics* 72 (2) (2007) 140–162.
- [20] G. F. Oster, J. D. Murray, Pattern formation models and developmental constraints, *Journal of Experimental Zoology* 251 (2) (1989) 186–202.
- [21] Z. Wang, T. Hillen, Classical solutions and pattern formation for a volume filling chemotaxis model, *Chaos: An Interdisciplinary Journal of Nonlinear Science* 17 (3) (2007) 037108–037108.
- [22] K. J. Painter, T. Hillen, Volume-filling and quorum-sensing in models for chemosensitive movement, *Can. Appl. Math. Quart* 10 (4) (2002) 501–543.
- [23] M. Mimura, T. Tsujikawa, Aggregating pattern dynamics in a chemotaxis model including growth, *Physica A: Statistical Mechanics and its Applications* 230 (3) (1996) 499–543.
- [24] T. Hillen, K. Painter, Global existence for a parabolic chemotaxis model with prevention of overcrowding, *Advances in Applied Mathematics* 26 (4) (2001) 280–301.
- [25] M. Myerscough, P. Maini, K. Painter, Pattern formation in a generalized chemotactic model, *Bulletin of mathematical biology* 60 (1) (1998) 1–26.
- [26] K. Osaki, T. Tsujikawa, A. Yagi, M. Mimura, Exponential attractor for a chemotaxis-growth system of equations, *Nonlinear Analysis: Theory, Methods & Applications* 51 (1) (2002) 119–144.
- [27] M. Aida, M. Efendiev, A. Yagi, Quasilinear abstract parabolic evolution equations and exponential attractors, *Osaka Journal of Mathematics* 42 (1) (2005) 101–132.
- [28] K. Painter, T. Hillen, Spatio-temporal chaos in a chemotaxis model, *Physica D: Nonlinear Phenomena* 240 (4) (2011) 363–375.
- [29] M. Ma, C. Ou, Z. Wang, Stationary solutions of a volume-filling chemotaxis model with logistic growth and their stability, *SIAM Journal on Applied Mathematics* 72 (3) (2012) 740–766.
- [30] T. Hillen, J. Zielinski, K. Painter, Merging-emerging systems can describe spatio-temporal patterning in a chemotaxis model, *Discrete and Continuous Dynamical Systems - B* .
- [31] Flexpde is a general-purpose commercial package to solve pde’s, see [www.pdesolutions.com](http://www.pdesolutions.com) .
- [32] Y. Nishiura, D. Ueyama, A skeleton structure of self-replicating dynamics, *Physica D: Nonlinear Phenomena* 130 (1) (1999) 73–104.

- [33] T. Kolokolnikov, M. Ward, J. Wei, Self-replication of mesa patterns in reaction–diffusion systems, *Physica D: Nonlinear Phenomena* 236 (2) (2007) 104–122.
- [34] M. Van Dyke, *Perturbation methods in fluid mechanics*, Vol. 964, Academic Press New York, 1964.
- [35] E. Hinch, *Perturbation methods*, Cambridge University Press, 1991.
- [36] A. Alcolado, T. Kolokolnikov, D. Iron, Instability thresholds in the microwave heating model with exponential nonlinearity, *European Journal of Applied Mathematics* 22 (03) (2011) 187–216.
- [37] D. Iron, M. Ward, J. Wei, The stability of spike solutions to the one-dimensional gierer–meinhardt model, *Physica D: Nonlinear Phenomena* 150 (1) (2001) 25–62.
- [38] A. Doelman, R. Gardner, T. Kaper, Stability analysis of singular patterns in the 1d gray-scott model: a matched asymptotics approach, *Physica D: Nonlinear Phenomena* 122 (1) (1998) 1–36.
- [39] J. Wei, On single interior spike solutions of the gierer-meinhardt system: uniqueness and spectrum estimates, *European Journal of Applied Mathematics* 10 (4) (1999) 353–378.
- [40] H. Van der Ploeg, A. Doelman, Stability of spatially periodic pulse patterns in a class of singularly perturbed reaction-diffusion equations., *Indiana University mathematics journal* 54 (5) (2005) 1219–1301.
- [41] R. McKay, T. Kolokolnikov, Stability transitions and dynamics of localized patterns near the shadow limit of reaction-diffusion systems, *Discrete and Continuous Dynamical Systems B*, to appear (2012) 171.